Journal of Systems Engineering and Electronics
Vol. 32, No. 5, October 2021, pp.1130 – 1142

Quasi-LFM radar waveform recognition based on fractional Fourier transform and time-frequency analysis

XIE Cunxiang[1], ZHANG Limin[1], and ZHONG Zhaogen[2,*]

1. Department of Information Fusion, Naval Aviation University, Yantai 264001, China;
2. School of Aviation Basis, Naval Aviation University, Yantai 264001, China

Abstract: Recent advances in electronics have increased the complexity of radar signal modulation. The quasi-linear frequency modulation (quasi-LFM) radar waveforms (LFM, Frank code, P1–P4 code) have similar time-frequency distributions, and it is difficult to identify such signals using traditional time-frequency analysis methods. To solve this problem, this paper proposes an algorithm for automatic recognition of quasi-LFM radar waveforms based on fractional Fourier transform and time-frequency analysis. First of all, fractional Fourier transform and the Wigner-Ville distribution (WVD) are used to determine the number of main ridgelines and the tilt angle of the target component in WVD. Next, the standard deviation of the target component's width in the signal's WVD is calculated. Finally, an assembled classifier using neural network is built to recognize different waveforms by automatically combining the three features. Simulation results show that the overall recognition rate of the proposed algorithm reaches 94.17% under 0 dB. When the training data set and the test data set are mixed with noise, the recognition rate reaches 89.93%. The best recognition accuracy is achieved when the size of the training set is taken as 400. The algorithm complexity can meet the requirements of real-time recognition.

Keywords: quasi-linear frequency modulation (quasi-LFM) radar waveform, time-frequency distribution, fractional Fourier transform (FrFT), assembled classifier.

DOI: 10.23919/JSEE.2021.000097

1. Introduction

Recognizing the waveform of radar signals plays a key role in electronic warfare. Lots of research around the world has been devoted to the problem of being able to recognize radar signal waveforms [1−3]. Early recognition algorithms depend on time-domain, frequency-domain [4,5] and high-order statistical analysis [6−8] of radar signals. A radar signal modulation recognition method was proposed in [9], based on spectrum complexity that achieves a recognition rate greater than 90% at a signal-to-noise ratio (SNR) of 6 dB, but the overall recognition rate is very low at a low SNR. In [10], a frequency estimator was used to obtain the instantaneous frequency characteristics of binary phase-shift keying (BPSK), quadrature amplitude modulation (QAM), and phase-shift keying (PSK) signals. However, this method can only identify certain special signals and is not universal. A method based on random projection and sparse classification was proposed in [11], to identify radar signal waveforms. First, the signal is compressed by random projections, and then the compressed signal is identified by the sparse classification (SC) algorithm. With six kinds of radar signals, the overall recognition rate reaches 90% at an SNR of 0 dB. However, one-dimensional time-domain or frequency-domain analysis cannot accurately reflect the time-varying characteristics of non-stationary signals that arise with the increased complexity of recently developed radar intra-pulse modulation methods. As a result, analyzing and recognizing radar signals in the time-frequency domain and transform-domain have become a focus of recent research. In [12] and [13], short-time Fourier transform (STFT) methods were used to analyze and recognize linear frequency modulation (LFM) signals, frequency shift keying (FSK) signals, PSK signals, and continuous wave signals. This approach produced an overall recognition accuracy of 90% for an SNR of 0 dB. A fractional Fourier transform (FrFT) approach was adopted in [14], based upon a chirp-based sparse decomposition of radar signals. Here, an overall recognition accuracy of 95% was achieved for an

Manuscript received December 16, 2020.
*Corresponding author.
This work was supported by the National Natural Science Foundation of China (91538201), the Taishan Scholar Project of Shandong Province (ts201511020), and the project supported by Chinese National Key Laboratory of Science and Technology on Information System Security (6142111190404).

SNR of −3 dB. However, this method was only able to classify signals into five categories, according to the chirp-based parameters. When the number of different types of signal increases, this method will experience a significant reduction in the recognition rate. To deal with cross-term interference in the Wigner-Ville distribution (WVD), which plays an important part in time-frequency analysis, a Choi-Williams distribution (CWD) was used for feature extraction and the recognition of radar waveforms. In [15], the singular value entropy from the CWD of eight types of radar waveforms was extracted. The box and information dimensions of the signal spectrum were then extracted, before applying a support vector machine (SVM) to bring about signal recognition. Here, the overall recognition rate reached 95% for an SNR higher than 1 dB. In [16], features were extracted from the CWD of the signal through image filtering, skeleton extraction, principal component analysis (PCA), image Binarization algorithm, Pseudo-Zernike moments, etc. Subsequently, Elman neural network (ENN) was used to classify different radar waveforms. The overall recognition rate achieved using this method was greater than 94% at an SNR of −2 dB. In [17], a radial integration method based on the integral rotation factor was proposed to detect six kinds of radar waveforms, namely, frequency-modulated continuous wave (FMCW), BPSK, Costas code, Frank code, P1 code, P2 code signals in the CWD. However, the recognition accuracy of the algorithm is not satisfactory at a low SNR. Deep learning (DL) is a method based on representational learning of data, which can adaptively select features, thereby effectively overcoming the disadvantages of artificially set features [18,19]. Many scholars have also utilized this method for recognizing the radar waveforms. Convolutional neural networks (CNNs) are deep learning methods, widely used for image recognition [20,21], speech recognition [22,23], computer vision [24], hand writing recognition [25], etc. They can extract deep-level features and can improve the recognition accuracy. In [26], CNN was used to extract features from the CWD of the signal to identify eight different radar waveforms, namely, LFM, BPSK, Costas codes, Frank codes, and polytime codes (T1, T2, T3, T4). The simulation results show that the overall recognition rate reached 93.7% at an SNR of −2 dB.

It can be seen from the state-of-the-art that the method of time-frequency analysis is widely used for radar waveforms recognition. Artificially predefined feature extraction methods and CNNs are the two broad categories of methods used to extract feature parameters from the time-frequency distribution of the signal. Finally, a classifier is used to identify different radar waveforms. However, for quasi-LFM radar waveforms (LFM, Frank code, P1−P4 code), the time-frequency distributions are similar, which poses difficulties in using the traditional time-frequency analysis methods for identification. In this paper a method based on FrFT and time-frequency analysis is proposed to identify such signals. First, an FrFT is applied on the signal to determine the number of main ridgelines and the tilt angle of the target component in WVD. Then, the standard deviation of the target component's width in the signal's WVD is calculated. Finally, an assembled classifier using neural network is built that adopts the fusion algorithm to recognize different waveforms by automatically combining the three features. Simulation results verify the proposed algorithm's recognition accuracy, robustness, and algorithm complexity. Moreover, the proposed algorithm is compared with the existing algorithm proposed in [16] and [26] to demonstrate its superiority.

2. Quasi-LFM radar signal model

The mathematical model of quasi-LFM signals is as follows [27]:

$$x(t) = A\mathrm{e}^{\mathrm{j}(2\pi f_c t+\phi_i)} \tag{1}$$

where A represents the amplitude, f_c represents the carrier frequency, and ϕ_i represents the modulation phase. The six types of quasi-LFM signals discussed in this paper differ in terms of the modulation phase. The specific mathematical models for each of the six types are shown in Table 1, in which $m = 1,2,\cdots,M$; $n = 1,2,\cdots,N$; $M = \sqrt{N_c}$; and $k = 1,2,\cdots,N_c$.

Table 1 Modulation phase of six kinds of quasi-LFM signals

Code type	Definition of ϕ_i
LFM	$\phi = \pi\mu t^2$
Frank	$\phi_{mn} = 2\pi(m-1)(n-1)/M$
P1	$\phi_{mn} = -\pi[M-(2n-1)][(n-1)M+(m-1)]/M$
P2	$\phi_{mn} = -\pi(2n-1-M)(2m-1-M)/2M$
P3	$\phi_k = \pi(k-1)^2/N_c$
P4	$\phi_k = \pi(k-1)^2/N_c - \pi(k-1)$

It is assumed that N_c= 256, the signal amplitude is $A = 1$, the carrier frequency is f_c=3 000 Hz, and the sampling frequency is f_s=12 000 Hz. The LFM, Frank code, P1 code, P2 code, P3 code, and P4 code WVDs are shown in Fig. 1.

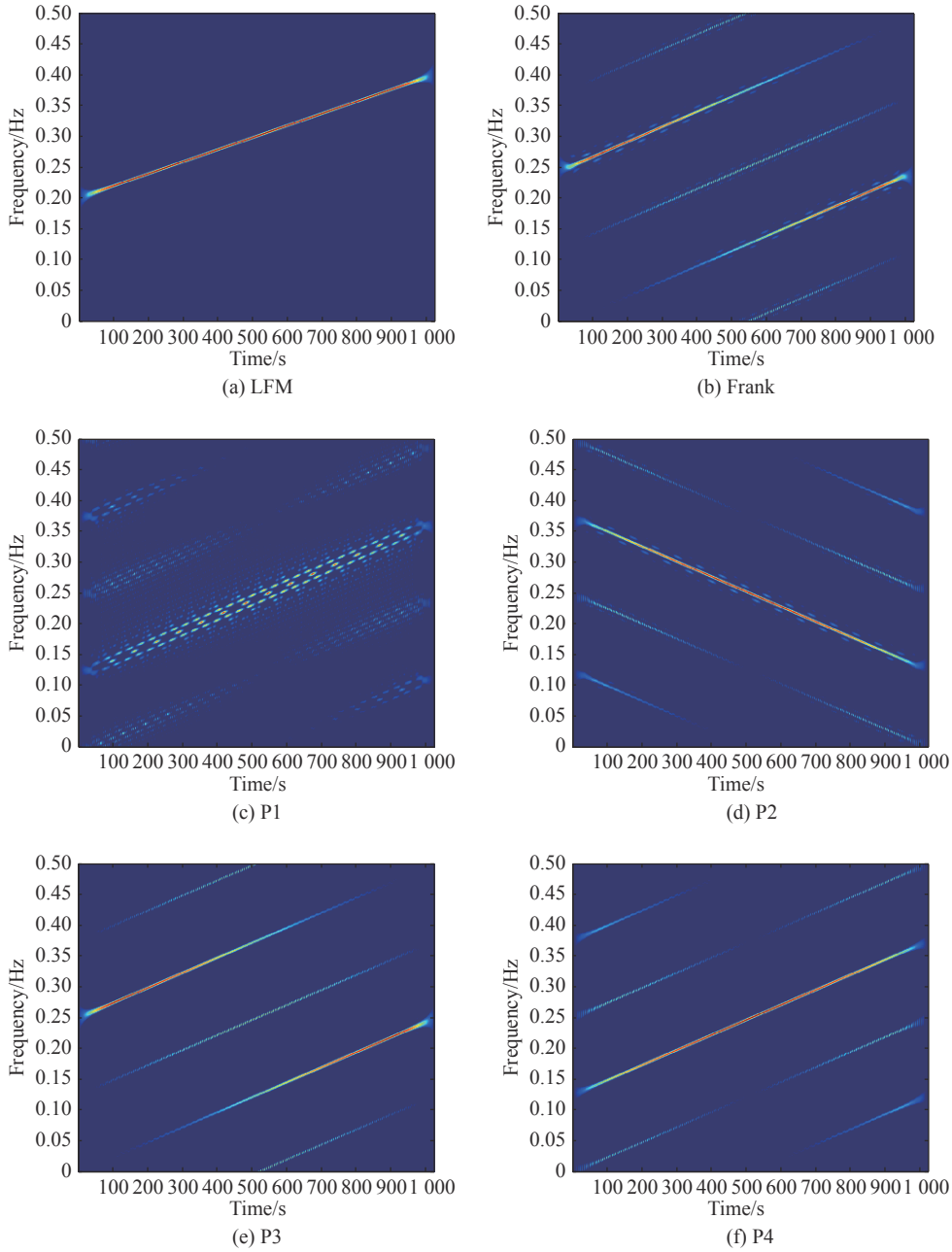

Fig. 1 WVDs for six types of quasi-LFM signals

3. Time-frequency feature extraction

3.1 FrFT

An FrFT takes the following form [28]:

$$X_p(u)=\int_{-\infty}^{\infty}K_p(u,t)\,x(t)\,\mathrm{d}t. \tag{2}$$

The transformation kernel function $K_p(u,t)$ can be defined as follows:

$$K_p(u,t)=\begin{cases}A_\alpha \mathrm{e}^{\mathrm{j}\pi\left[\left(u^2+t^2\right)\cot\alpha-2ut\csc\alpha\right]}, & \alpha\neq n\pi\\ \delta(t-u), & \alpha=2n\pi\\ \delta(t+u), & \alpha=(2n+1)\pi\end{cases} \tag{3}$$

where p represents the fractional order, $\alpha=p\pi/2$ represents the fractional rotation angle, and $A_\alpha=\sqrt{1-\mathrm{j}\cot\alpha}$.

The essence of the FrFT is the chirp basis decomposition [29]. Therefore, FrFT has good time-frequency energy accumulation characteristics for quasi-LFM signals.

Moreover, the relationship between an FrFT and the WVD is demonstrated in [29], which can be described as the WVD of a signal's FrFT is the rotated coordinate form of the original signal's WVD, with the direction of rotation being counterclockwise and the rotation angle being equal to the fractional rotation angle.

3.2 Signal characteristics in the fractional domain

The WVDs of the quasi-LFM signals shown in Fig.1 are all inclined straight lines at a certain angle to the time domain axis. Let us assume that the angle between the straight line and the time domain axis is β. According to the relationship between the FrFT and the WVD obtained in Section 3.1, as long as the rotation angle of the FrFT, α, and β are orthogonal, signal energy aggregation will occur in a narrow band of the fractional domain, as shown in Fig. 2.

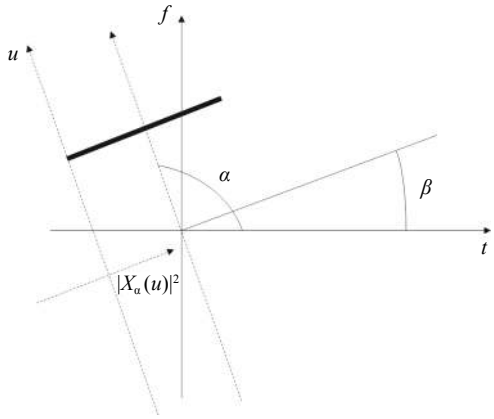

Fig. 2 Signal energy aggregation in the fractional domain

In practical applications, the inclination angle, β, of a signal's WVD cannot be known in advance, so it is necessary to use the rotation angle, α, as a variable to perform an FrFT on the observed signal. This gives the energy distribution of the signal in different fractional domains, thereby providing the two-dimensional distribution of the signal energy on the plane (α, u). By conducting a two-dimensional search of the signal energy, the energy peak value and the corresponding rotation angle α_0, and the fractional domain frequency u_0 can be described as

$$\{\alpha_0, u_0\} = \arg\max_{\alpha,u} |X_\alpha(u)|^2. \tag{4}$$

Then the optimal fractional order p_0 can be obtained as $p_0 = 2\alpha_0/\pi$.

Taking the Frank code as an example, the two-dimensional distribution of signal energy on the plane (α, u) is shown in Fig. 3.

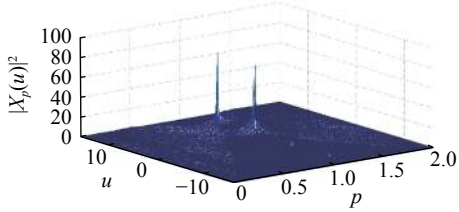

Fig. 3 Two-dimensional distribution of Frank code signal energy on the plane (α, u)

According to the energy aggregation of the quasi-LFM signals in the fractional domain in Fig. 2, we can get that

$$\begin{cases} \mu = -\cot\alpha_0 \\ f_c = u_0 \csc\alpha_0 \end{cases} \tag{5}$$

where μ and f_c represent the modulation frequency and the carrier frequency of the quasi-LFM signal, respectively. Considering that the modulation frequency and the carrier frequency of the Frank code signal are both positive, then we can get that $\pi/2 < \alpha_0 < \pi (1 < p_0 < 2)$ and $u_0 > 0$.

By performing an FrFT with a rotation angle of α_0, the corresponding energy distribution in the best fractional domain is shown in Fig. 4.

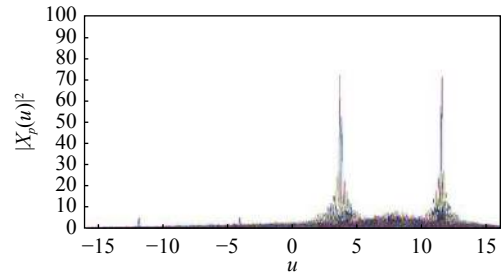

Fig. 4 Frank code signal energy distribution in the best fractional domain

It can be seen from Fig. 4 that the Frank code signal has two energy peaks in the best fractional domain, which correspond to the two main ridges in the WVD. Therefore, the number of main ridges in the WVD of the signal can be judged according to the energy peak in the best fractional domain of the signal. At the same time, Fig. 1 shows that only the P2 code signal corresponds to the fractional rotation angle, $\alpha < \frac{\pi}{2}$, with the other signals corresponding to the fractional rotation angle $\alpha > \frac{\pi}{2}$. All the above characteristics can be used for signal classification. The specific algorithm for this is as follows:

(i) Take the rotation angle, α, as a variable and perform an FrFT on the observed signal to obtain the two-dimensional distribution of the signal energy on the plane (α, u).

(ii) Perform a two-dimensional search on the signal energy to obtain the fractional rotation angle, α, corresponding to the peak energy. If $\alpha < \frac{\pi}{2}$, the signal can be regarded as a P2 code signal. Conversely, perform an FrFT on the signal with the fractional rotation angle, α, to obtain the energy distribution of the signal in the best fractional domain.

(iii) Call the signal energy peak in the best fractional domain E, then select the location points $u_1, u_2, \cdots, u_k$ where the energy value is greater than $0.6E$

and calculate the average value, $u_0 = \frac{1}{k}\sum_{i=1}^{k} u_i$. According to the average value, u_0, divide the location points into two parts, U_1 and U_2. U_1 incorporates the points that are less than u_0; U_2 incorporates the points that are greater than u_0. Calculate the corresponding mean values, u' and u'', respectively.

(iv) Calculate $r = \frac{u'}{u''}$. If $r \leqslant 0.5$, it indicates that the WVD of the signal has two main ridges. If $r > 0.5$, it indicates that the WVD of the signal has one main ridge.

The classification of six types of quasi-LFM signals based on the above algorithm is shown in Fig. 5.

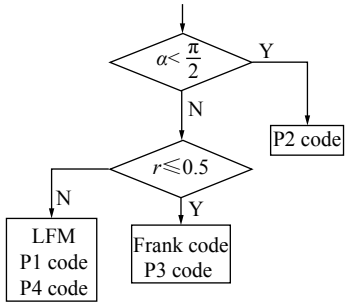

Fig. 5 Signal classification process based on the FrFT algorithm

3.3 Standard deviation of target component width in WVD

The identification of quasi-LFM radar waveforms from the number of main ridgelines and from the tilt angle of the target component in WVD has the following limitations:

(i) LFM, P1 code signal and P4 code signal cannot be distinguished.

(ii) Frank code signal cannot be distguished from the P3 code signal.

As shown in Fig. 1, Frank, P1 and P2 code signals are uneven curves with obvious blocky structures as they are based on frequency approximations of an LFM signal. P3 and P4 code signals have smoother curves because they are sampled from an LFM signal. The LFM signal has the smoothest curves and contains no additional components [30]. This feature is reflected by the standard deviation of the target component width.

However, the target component is at a certain angle to the time domain axis, which makes the direct calculation difficult. The calculation of the standard deviation of the target component becomes easier if the time-frequency image is rotated so that the target component is parallel either to the time domain axis or to the frequency domain axis. However, this rotation process requires additional computations for calculating the interpolation.

The WVD of the signal $x(t)$ is rotated counterclockwise by an angle of θ ($\theta = p\pi/2$), to obtain $X_p(u)$, which is the FrFT of $x(t)$. Therefore, the FrFT of the signal $x(t)$ with a specific fractional order p, makes the target component in the WVD of $X_p(u)$ parallel to the time domain axis. This algorithm reduces the difficulty in calculating the standard deviation of the target component, and it can also reduce the number of computations needed for rotating the time-frequency distribution.

The signal parameters are the same as those mentioned in Section 2, and an FrFT with a specific fractional order p is performed on the quasi-LFM signals. The WVD is shown in Fig. 6, in which the target component is parallel to the time domain axis.

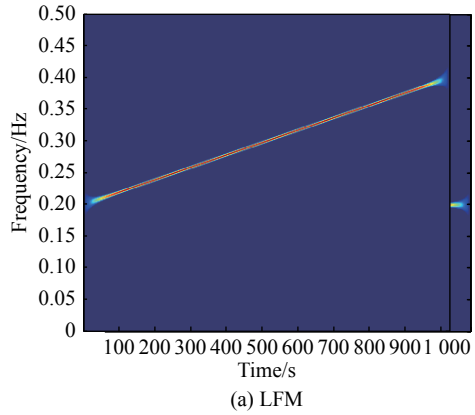

(a) LFM

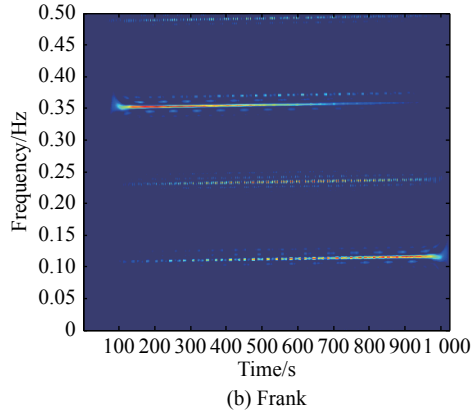

(b) Frank

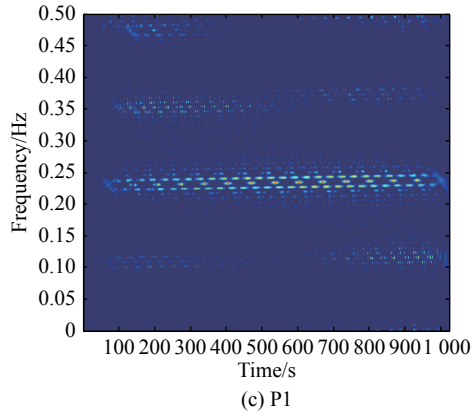

(c) P1

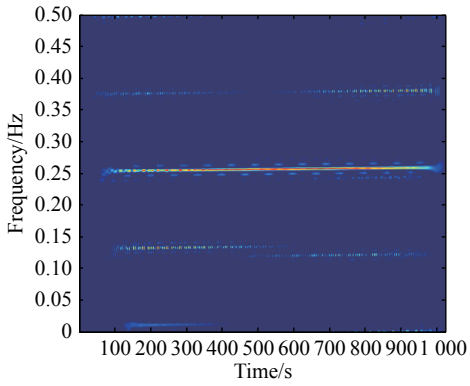

(d) P2

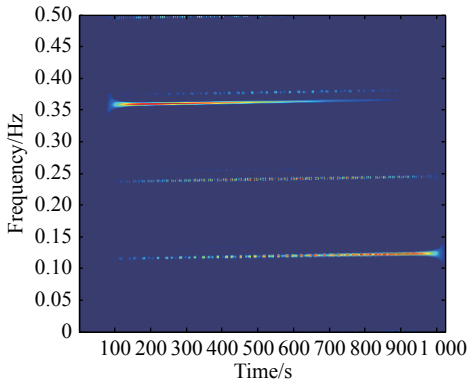

(e) P3

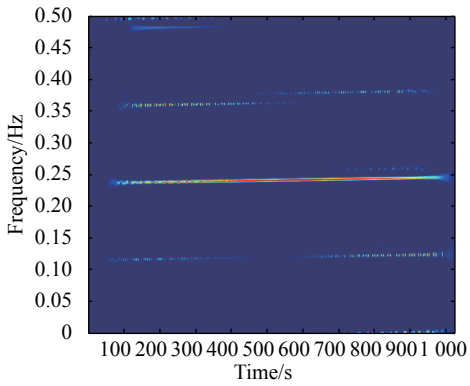

(f) P4

Fig. 6 WVD for the six different quasi-LFM signals after an FrFT

The specific fractional order p has to be determined. According to the assumption mentioned in Section 3.2, if the WVD of the signal $x(t)$ is rotated counterclockwise by an angle of β, then the target component becomes parallel to the time domain axis. Therefore, the FrFT is applied to the signal $x(t)$ so as to obtain $X_p(u)$ by rotating its WVD by an angle of β ($\beta = p\pi/2$). This makes the target component in the WVD of $X_p(u)$ parallel to the time domain axis. In accordance with the description given in Section 3.2, to determine the angle β between the target component and the time domain axis, a two-dimensional search is conducted on the signal energy. From this two-dimensional search, the energy peak value and the corresponding rotation angle, α, can be obtained. α is orthogonal to β, so β can be determined as

$$\beta = \begin{cases} \alpha - \dfrac{\pi}{2}, & \alpha \geqslant \dfrac{\pi}{2} \\ \alpha + \dfrac{\pi}{2}, & \alpha < \dfrac{\pi}{2} \end{cases}. \tag{6}$$

Then the specific fractional order can be calculated as $p = 2\beta/\pi$.

The above-mentioned time-frequency image needs to be binarized to eliminate the influence of independent noise points. The binarized image is essentially a two-dimensional matrix $\boldsymbol{B}(i, j)$, where i and j can take integer values $1, 2, \cdots, M$. The sum of the rows of the matrix are given by $D(i) = \sum_{j=0}^{M-1} \boldsymbol{B}(i, j)$, where $i = 1, 2, \cdots, M$. As the target value is 1 and the background value is 0 after the binarization process, $D(i)$ represents the width of the target component with respect to the time domain axis.

Normalizing $D(i)$ to maintain its value between 0 and 1, we get

$$\hat{D}(i) = \frac{D(i)}{\max D(i)}. \tag{7}$$

Then the standard deviation of the target component width can be calculated as follows:

$$\sigma = \sqrt{\frac{1}{M}\sum_{i=0}^{M-1} \hat{D}^2(i) - \left(\frac{1}{M}\sum_{i=0}^{M-1} \hat{D}(i)\right)^2}. \tag{8}$$

4. Assembled neural network classifier design

The neural network has the ability to learn by itself. It can analyze the underlying laws between the input and the output data, provided during its training phase. Finally, it uses these laws to predict the output for a given input [31]. Therefore, it is a good choice to use a neural network to identify different radar waveforms.

According to the signal features described in Section 3, the quasi-LFM radar waveforms can be identified by using these features. However, these features need to be effectively integrated to improve the overall recognition performance. In order to achieve multi-feature fusion, and to overcome the problem of overfitting [32], an assembled neural network has to be used as a signal classifier.

An assembled classifier model using neural networks is

composed of system inputs, single neural network design, combination structures, and fusion principles [32], as shown in Fig.7.

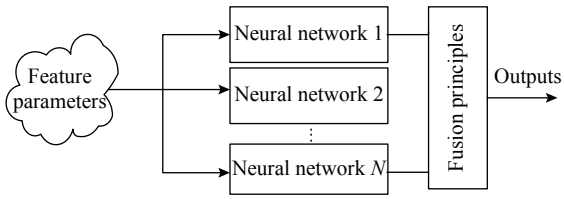

Fig. 7 Assembled neural network classifier model

The back propagation (BP) neural network is widely used in machine learning. The mathematical theory has proved that a three-layer BP neural network can fit any kind of nonlinear function with arbitrary precision, and has a strong ability to nonlinearly map the inputs to the outputs [33]. The radial basis function (RBF) neural network is a kind of local approaching neural network that can adaptively determine the radial neurons and has a fast convergence speed. In this paper different neural networks based on BP and RBF are used for the waveform classification.

The numbers of neurons in the input layer and in the output layer are determined by the number of features and by the number of waveforms, respectively. There are three feature parameters and six waveforms for each classifier.

The performance of the assembled classifier depends heavily on fusion principles. Several fusion algorithms have been proposed such as the majority vote algorithm, the simple average algorithm, the optimal linear combination algorithm, and the confidence factor algorithm [34]. The output of a trained neural network can be an approximate posterior probability. In this paper the waveforms are recognized through the majority vote algorithm which utilizes weighted posterior probabilities.

Assume the number of the waveforms that are classified to be K, the number of the classifiers to be N and the input feature vector to be $\boldsymbol{X}$. The kth output of the nth classifier is

$$O_{nk}(\boldsymbol{X}) = P(c_k|\boldsymbol{X}) + e_{nk}(\boldsymbol{X}) \tag{9}$$

where $P(c_k|\boldsymbol{X})$ is the posterior probability that $\boldsymbol{X}$ is classified as the kth type of waveform; $e_{nk}(\boldsymbol{X})$ is the output error of the k th node in the n th classifier. Assuming $\boldsymbol{\omega}_{nk} = \{\omega_{1k}, \omega_{2k}, \cdots, \omega_{Nk}\}$ to be the kth output weight of the nth classifier, the summation of the weighted outputs that each classifier classifies as the same type is

$$S_k(\boldsymbol{X}) = \sum_{n=1}^{N} \omega_{nk} O_{nk}(\boldsymbol{X}) \tag{10}$$

with the restriction that $\sum_{n=1}^{N} \omega_{nk} = 1$ and $\sum_{n=1}^{N} \omega_{nk} e_{nk}(\boldsymbol{X}) = 0$, then

$$S_k(\boldsymbol{X}) = P(c_k|\boldsymbol{X}). \tag{11}$$

When $S_k = \max\limits_{1 \leqslant j \leqslant K} S_j$, the kth type of waveform could be recognized.

5. Simulation and analysis

5.1 Simulated signal generation

Targeting the six quasi-LFM radar signals mentioned above, the feature extraction algorithm proposed in Section 3 was verified by using Matlab simulations.

For each of these six quasi-LFM radar signals, 1 000 samples with different SNRs were generated. The characteristics of the samples were obtained by using the proposed feature extraction algorithm. Out of these 1 000 samples, 800 were used for training, and the remaining 200 were used for testing. Ten different simulations were performed by using the same data and the recognition rates were calculated. The final signal recognition rate was taken as the average of these ten recognition rates.

The generated signals had the following specific parameters: the sampling frequency was 12 000 Hz and the carrier frequency was evenly distributed between 3 000 Hz and 3 500 Hz. There were N ranges from 4 to 8 for the Frank code and P1 code signals. The P2 code signal had the values of 6 and 8. The signal pulse compression ratio ρ of the P3 code and the P4 code was $N \times N$, where $N \in [4, 8]$. The symbol rate was one-fourth of the carrier frequency. The signal samples were generated with an SNR of −6 dB, −4 dB, −2 dB, ⋯, 12 dB. The structure of the CNN and the specific parameters were taken to be the same as those presented in Section 4. Since BP network and RBF network have a faster convergence speed than other networks, four neural networks having different structures were used. These networks had independent initial statuses and training procedures to form an assembled neural network classifier. These neural networks are BP1(5-10-6), BP2(5-12-6), RBF1(5-10-6), RBF2(5-12-6). The initial weights were set randomly. When the recognition mean square error is less than 0.001, it can be considered as an effective recognition.

The experimental flow graph is shown in Fig. 8.

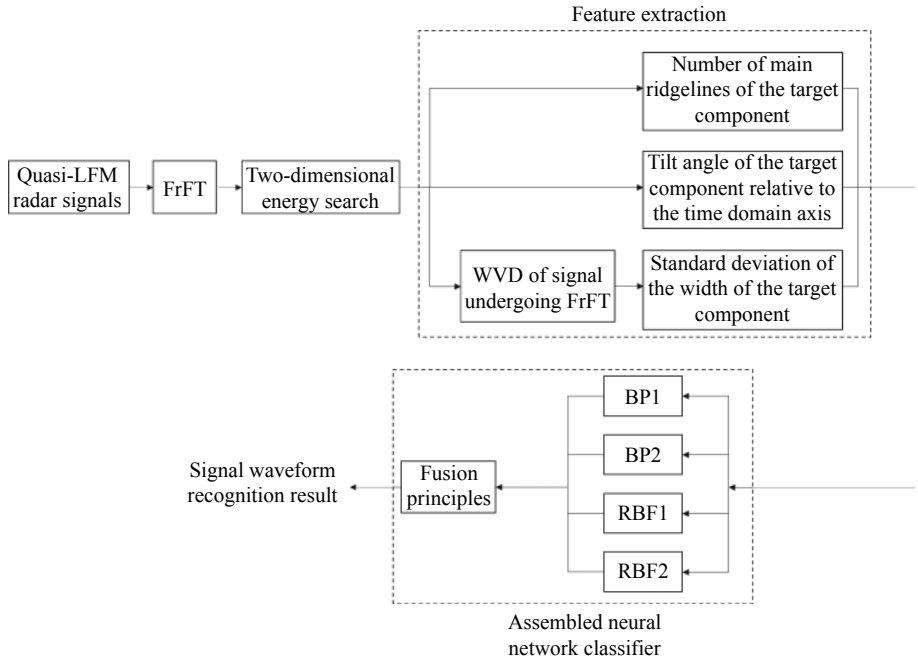

Fig. 8 Experimental flow graph

5.2 Recognition accuracy verification

The radar waveform recognition algorithm based on FrFT and time-frequency analysis proposed in this paper is simulated and verified. It is also compared with the other recognition algorithms available in [16,26] to demonstrate its supremacy.

Fig. 9 and Fig. 10 show the recognition rate and the overall recognition rate for the six quasi-LFM signals at different SNRs, respectively.

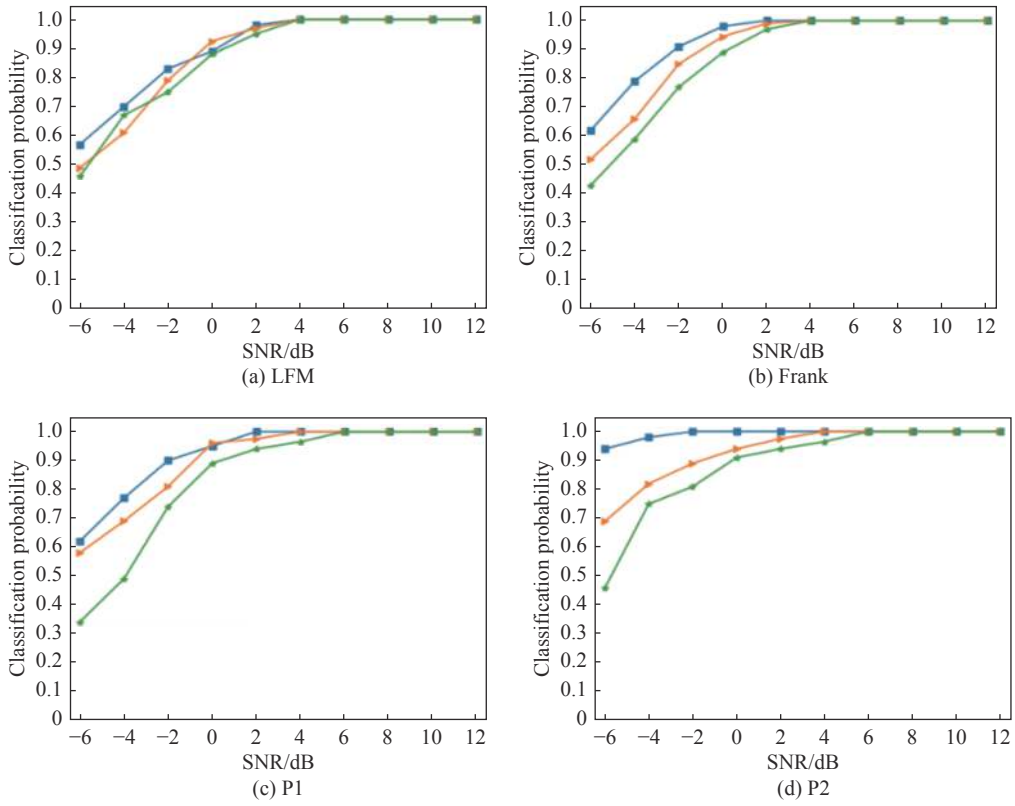

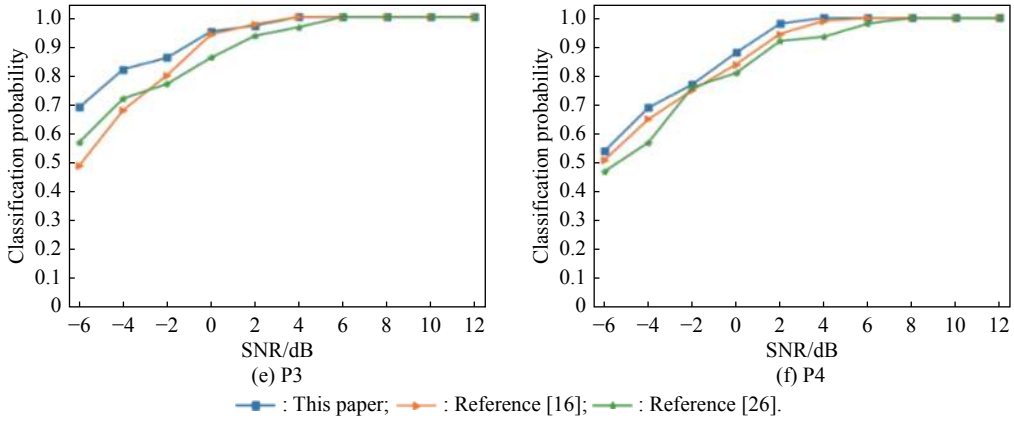

Fig. 9 Correct recognition rate for the six quasi-LFM signals

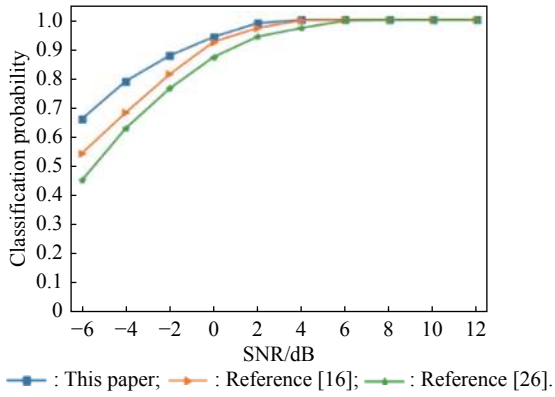

Fig. 10 Overall recognition rate

It can be seen from Fig. 9 that for each of the quasi-LFM signal, the recognition performance of the proposed algorithm is higher than the recognition performance of the algorithms proposed in [16,26]. This is especially true for the recognition of Frank codes and P2 codes. Thus, the proposed algorithm has obvious advantages.

It can be seen in Fig. 10 that by using the proposed algorithm for identifying the six different quasi-LFM signals, the overall recognition rate reaches 94.17% at an SNR of 0 dB, which is better than the recognition rates achieved by using the algorithms proposed in [16,26].

The confusion matrices for signal recognition at SNRs of −6 dB, −4 dB, −2 dB, 0 dB, and 2 dB are shown in Fig. 11. It can be seen from Fig. 11 that the recognition rate for the P2 code signal reaches 100% for all the SNRs considered. This is because the P2 code signal can be directly identified by the feature extraction algorithm based on the FrFT. The FrFT has good energy accumulation for the quasi-LFM signals and is robust against noise. This also demonstrates the superiority of the proposed feature extraction algorithm.

Nonetheless, some confusion did arise with low SNRs. For example, around 25% of the Frank codes were incorrectly classified as P3 codes at an SNR of −6 dB. Besides, roughly 41% of the P4 codes were incorrectly classified as LFM at −6 dB. Although in theory, the Frank code signal can be distinguished from the P3 code signal, and the LFM signal can be distinguished from the P4 code signal, based on the difference in the standard deviation of the target component width in WVD, at low SNRs, noise affects the time-frequency distribution. As a result, the proportion of non-target components increases, which affects the feature extraction and signal recognition process. This also gives the directions for improving the algorithm.

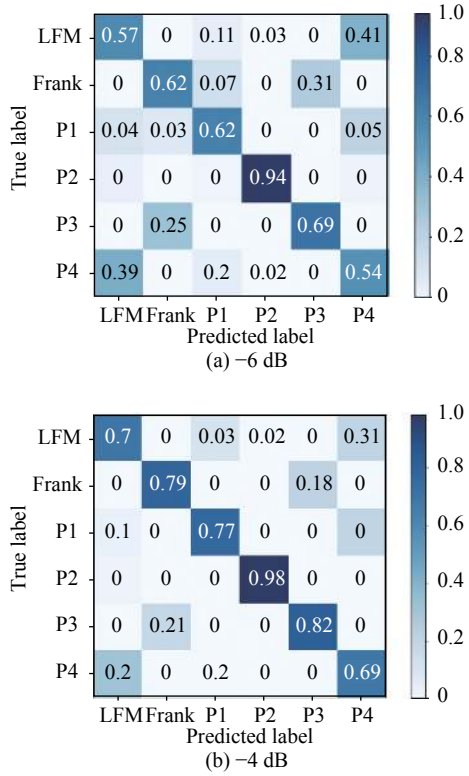

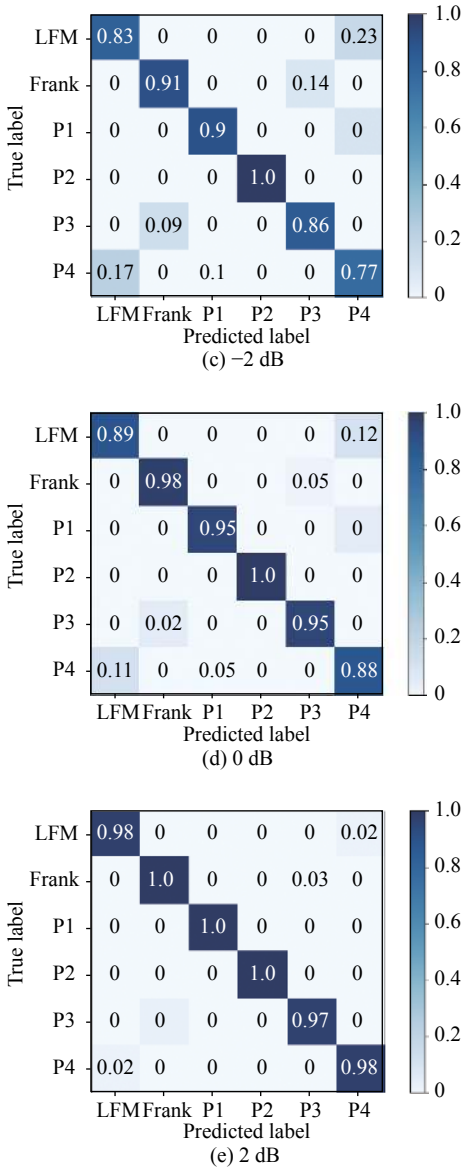

Fig. 11 Confusion matrices for signal recognition at SNRs of −6 dB, −4 dB, −2 dB, 0 dB, and 2 dB

5.3 Verification of the recognition robustness

In reality, the SNR of the received radar signals cannot be guaranteed to be the same, so it is necessary to mix signals with different SNRs for training and testing of the classifier. Besides, the number of samples used for training the neural network is an important factor to measure the recognition performance of the algorithm. A good algorithm does not require a large number of training samples to achieve efficient signal recognition. Therefore, we need to test the recognition rate by changing the number of training samples.

In summary, the recognition robustness was verified in two ways: (i) Sample signals were generated, the feature parameters were extracted for different SNRs, which were used for obtaining the recognition rate. (ii) The number of samples in the training set varied and the number of test samples was fixed to obtain the recognition rates.

First, the signal parameters were set in accordance with the values mentioned in Section 5.1. Two hundred signal samples each were generated at SNRs of −6 dB, −4 dB, −2 dB, 0 dB and 2 dB respectively. These 1 000 samples were mixed randomly to serve as the training set. Similarly, a further 40 signal samples were generated with the same SNRs and mixed randomly to obtain the test set (200 test samples). Finally, the signal recognition rate was obtained by using the assembled neural network, by mixing signals with different SNRs. The confusion matrix for the signal recognition is shown in Fig. 12. It can be seen from Fig. 12 that the overall signal recognition rate is 89.93%, and the signal recognition confusion matrix for mixed SNRs is similar to the confusion matrix for signal recognition at an SNR of −2 dB in Section 5.2. This indicates that the signal recognition model proposed in this paper does not have the problem of low recognition rates when processing and identifying mixed SNR signals. On the contrary, it can still achieve a high recognition rate, even with signals having different SNRs. This is attributed to the anti-noise performance of the feature extraction algorithm and the good classification performance of the classification network. On the one hand, the FrFT has good energy aggregation for quasi-LFM signals, so it can extract characteristic parameters accurately at high, medium and low SNRs. On the other hand, the assembled neural network classifier has a good adaptability to the characteristic parameters extracted from the same class of signals with different SNRs, so that the feature parameters can be determined as the same class.

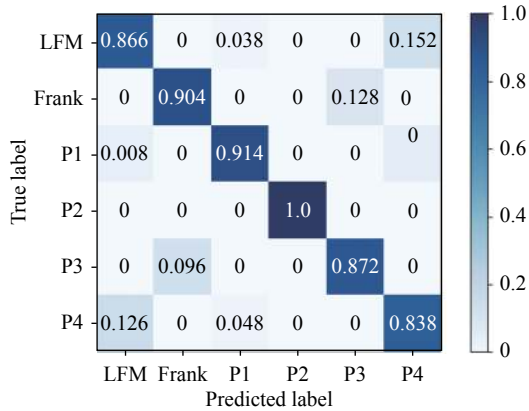

Fig. 12 Signal recognition confusion matrix for mixed SNRs

Then, for each radar signal, the number of training samples was increased from 100 to 500, in increments of

100 and the number of test samples was fixed at 200. The experiments were performed for SNRs of −6 dB, −4 dB,⋯, 12 dB, and the results are shown in Fig. 13.

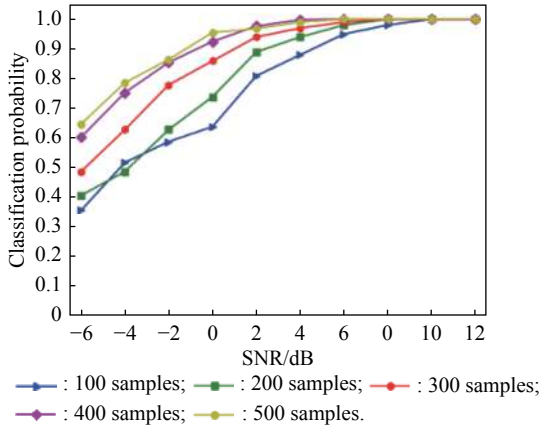

Fig. 13 Signal recognition rate for different numbers of training samples

Fig. 13 shows that, as the number of training samples increases, the signal recognition rate for different SNRs also increases. When the number of samples in the training set reaches 400, the signal recognition rate saturates. Therefore, the best recognition rates can be achieved by using the training set having 400 samples. This indicates that the proposed signal recognition model can work well in the small number of samples. This is because the feature parameters obtained through the feature extraction algorithm proposed in this paper can well reflect the characteristics of different types of signals. At the same time, the neural network has good nonlinear mapping and convergence performance. Therefore, the signal recognition model can accurately link the characteristic parameters of the signal with the category by training the network with only a few samples.

In summary, the simulation results confirm that the proposed algorithm is both robust and practically viable.

5.4 Algorithm complexity analysis

Algorithm complexity analysis includes three main parts: two-dimensional search for the signal energy through the FrFT, calculating the number of energy peaks in the fractional domain, and calculation of the target component width's standard deviation in WVD.

Assume that the number of sampling points per signal is N, and the discrete algorithm of the FrFT adopts the Pei sampling algorithm, the complexity for one calculation is $O(N\log_2 N)$. Assume that in the process of the two-dimensional search for the signal energy, the resolution of the fractional order p is Δp, and its range is between 0 and 2. Thus, the algorithm complexity for the two-dimensional search of the signal's energy is $O(2/\Delta p \cdot N\log_2 N)$.

Assume that the peak energy of the signal in the best fractional domain is E, and the number of points in the best fractional domain having energy greater than $0.6E$ is K $(K < N)$. The algorithm complexity for calculating the mean of all these points is $O(K)$. The algorithm complexity for dividing the points into U_1 and U_2 based on the mean value of the points is $O(K)$. The algorithm complexity for calculating the mean value of the points of U_1 and U_2 is $O(K)$. Finally, the number of energy peaks in the fractional domain is determined, so the overall algorithm complexity is $O(3K+1)$.

To calculate the standard deviation of the target component width in WVD, first the FrFT of the signal with a specific fractional order has to be calculated, whose algorithm complexity is $O(N\log_2 N)$. Next, the WVD of the fractional domain signal has to be calculated. Two-dimensional FFT can be used to simplify the calculation and reduce the complexity. The algorithm complexity is $O(N^2\log_2 N)$. Finally, the standard deviation of the target component width is calculated and the complexity is $O(3N+2)$.

In summary, the overall algorithm complexity is $O((P+N+1)N\log_2 N+3K+3N+3)$. When the signal sampling points are in the range of 128 to 1 024, and the resolution of the fractional order p is 0.01, then the overall algorithm complexity is in the range of 10^5 to 10^7, which meets the requirement of quasi-LFM radar waveforms real-time recognition.

6. Conclusions

This paper proposes a recognition algorithm that uses the FrFT and time-frequency analysis for recognizing six types of quasi-LFM radar signals. The algorithm works as follows. First, an FrFT and a two-dimensional energy peak search are performed to determine the number of main ridgelines and the tilt angle of the target component in WVD. This is done on the basis of the relationship between the WVD and the FrFT. After this, the signal can be divided into three categories: the first category consists of the LFM, the P1 code and the P4 code; the second category consists of the Frank code and the P3 code; the third category consists of the P2 code. Based on the presence of block structure in the target component and its smoothness, and by calculating the standard deviation of the target component width, signals in category 1, as well as category 2, can be distinguished from each other. To simplify the algorithm, this paper proposes to rotate the WVD by performing an FrFT on the signal to ensure that the target component in the rotated WVD is parallel to the time-domain axis, so that the standard deviation of the target component width can be calculated easily.

Simulations show that the overall signal recognition rate can reach 94.17% at an SNR of 0 dB, and this performance is better than the algorithms proposed in [16,26]. In particular, as the FrFT has good anti-noise properties, for P2 code signals, the recognition rate is greater than 90% at an SNR of −6 dB. For verifying the robustness, the assembled neural network was trained and tested with a data set having signals with mixed SNRs, and the overall signal recognition rate reached 89.93%. Fixing the number of samples in the test set, the recognition rate was the highest as the number of samples in the training set reached 400, after which, it remained stable. Thus, the robustness of the proposed algorithm was confirmed from two different perspectives. Finally, by analyzing the algorithm complexity, it can be concluded that this algorithm can meet the requirements of real-time signal recognition.

However, the proposed radar waveform recognition algorithm still has some limitations. Firstly, except the P2 code signal, the other quasi-LFM radar waveforms are still disturbed by noise at low SNRs. It is mainly affected by noise in the process of extracting the standard deviation of target component width in WVD. How to reduce the noise influence of this process is the direction of algorithm optimization in the following. Secondly, the recognition performance of the algorithm in complex wireless communication channels (multipath fading, Doppler shift, etc.) is not discussed. This is the direction of the next research, which can ensure the algorithm adapts to the quasi-LFM radar waveforms recognition task in different wireless communication channels.

References

[1] QU Z Y, WANG W Y, HOU C B, et al. Radar signal intrapulse modulation recognition based on convolutional denoising autoencoder and deep convolutional neural network. IEEE Access, 2019, 7: 112339–112347.

[2] THOKALA R K, DEERGHA R K. Automatic intrapulse modulation classification of advanced LPI radar waveforms. IEEE Trans. on Aerospace and Electronic Systems, 2017, 53(2): 901–914.

[3] LI D J, YANG R J, LI X B, et al. Radar signal modulation recognition based on deep joint learning. IEEE Access, 2020, 8: 48515–48528.

[4] NANDI A K, AZZOUZ E E. Algorithms for automatic modulation recognition of communication signals. IEEE Trans. on Communications, 1998, 46(4): 431–436.

[5] NANDI A K, AZZOUZ E E. Automatic analogue modulation recognition. Signal Processing, 1995, 46(2): 211–222.

[6] RAVIER P, AMBLARD P O. Wavelet packets and de-noising based on higher-order-statistics for transient detection. Signal Processing, 2001, 81(9): 1909–1926.

[7] SWAMI A, SADLER B M. Hierarchical digital modulation classification using cumulants. IEEE Trans. on Communications, 2000, 48(3): 416–429.

[8] DOBRE O A, BARNESS Y, SU W. Higher-order cyclic cumulants for high order modulation classification. Proc. of the Military Communications Conference, 2003: 112–117.

[9] LIU L T, DAI L J, CHEN T. Radar signal modulation recognition based on spectrum complexity. Journal of Harbin Engineering University, 2018, 39(6): 1081–1086. (in Chinese)

[10] ZHANG Y X, HONG R J, PAN P P, et al. Frequency-domain range sidelobe correction in stretch processing for wideband LFM radars. IEEE Trans. on Aerospace and Electronic Systems, 2017, 53(1): 111–121.

[11] MA J, HUANG G, MZUO W, et al. Robust radar waveform recognition algorithm based on random projections and sparse classification. IET Radar, Sonar & Navigatation, 2014, 8(4): 290–296.

[12] LOPEZ-RISUENO G, GRAJAL J, SANZ-OSORIO A. Digital channelized receiver based on time-frequency analysis for signal interception. IEEE Trans. on Aerospace and Electronic Systems, 2005, 41(3): 879–898.

[13] LOPEZ-RISUENO G, GRAJAL J, YESTE-OJEDA O. Atomic decomposition-based radar complex signal interception. IEE Proceedings—Radar, Sonar and Navigation, 2003, 150(4): 323–331.

[14] HUANG Y, LIU F, WANG Z Z. Chirp function sparse feature extraction and sorting of radar signals based on FRFT. Acta Aeronautica et Astronautica Sinica, 2013, 34(2): 393–400. (in Chinese)

[15] QU Z Y, MAO X J, HOU C B. Radar signal recognition based on singular value entropy and fractal dimension. Systems Engineering and Electronics, 2018, 40(2): 303–307. (in Chinese)

[16] ZHANG M, LIU L T, DIAO M. LPI radar waveform recognition based on time-frequency distribution. Sensors, 2016, 16(10): 1682.

[17] LI Y J, XIAO P, WU H C, et al. LPI radar signal detection based on radial integration of Choi-Williams time-frequency image. Journal of Systems Engineering and Electronics, 2015, 26(5): 973–981.

[18] LECUN Y, BENGIO Y, HINTO G. Deep learning. Nature, 2015, 521(7553): 436–444.

[19] O'SHEA T, HOYDIS J. An introduction to deep learning for the physical layer. IEEE Trans. on Cognitive Communications and Networking, 2017, 3(4): 563–575.

[20] LAWRENCE S, GILES C L, TSOI A C, et al. Face recognition: a convolutional neural network approach. IEEE Trans. on Neural Networks, 1997, 8(1): 98–113.

[21] LECUN Y, HUANG F J, BOTTOU L. Learning methods for generic object recognition with invariance to pose and lighting. Proc. of the IEEE Computer Vision and Pattern Recognition, 2004, 2: 97–104.

[22] ABDEL-HAMID O, MOHAMED A R, JIANG H, et al. Applying convolutional neural networks concepts to hybrid NN-HMM model for speech recognition. Proc. of the IEEE International Conference on Acoustics, 2012: 4277−4280.

[23] ABDEL-HAMID O, MOHAMED A R, JIANG H, et al. Convolutional neural networks for speech recognition. IEEE/ACM Trans. on Audio, Speech and Language Processing, 2014, 22(10): 1533–1545.

[24] LIN T Y, ROYCHOWDHURY A, MAJI S. Bilinear CNN models for fine-grained visual recognition. Proc. of the IEEE International Conference on Computer Vision, 2015: 1449−1457.

[25] NIU X X, SUEN C Y. A novel hybrid CNN–SVM classifier for recognizing handwritten digits. Pattern Recognition, 2012, 45(4): 1318–1325.

[26] ZHAN M, DIAO M, GUO L M. Convolutional neural networks for automatic cognitive radio waveform recognition. IEEE Access, 2017, 5: 11074–11082.
[27] PACE P E. Detecting and classifying low probability of intercept radar. 3rd ed. New York: Artech House, 2009.
[28] DENG B, WANG X, TAO R, et al. Performance analysis of time delay estimation for linear frequency-modulated pulse based on fractional Fourier transform. Acta Armamentarii, 2012, 33(6): 764–768. (in Chinese)
[29] ALMEIDA L B. The fractional Fourier transform and time-frequency representation. IEEE Trans. on Signal Processing, 1994, 42(11): 3084–3091.
[30] LUNDEN J, TERHO L, KOIVUNEN V. Classifying pulse compression radar waveforms using time-frequency distributions. Proc. of the 39th Annual Conference on Information Sciences and Systems, 2005: 1−6.
[31] MONTAVON G, SAMEK M, MULLER K R. Methods for interpreting and understanding deep neural networks. Digital Signal Processing, 2018, 73: 1–15.
[32] WANG Y C, HU Z Y, ZHANG Y F. Digital modulated signal recognition based on spectral correlation and assembled neural network. Application Research of Computers, 2009, 26(11): 4234–4236. (in Chinese)
[33] WANG H J, NEIMULE M, JIN T. Application of adaptive genetic BP model in classification of speech characteristic signal. Proc. of the 2nd IEEE Advanced Information Management, Communicates, Electronic and Automation Control Conference, 2018: 1429−1433.
[34] MILLER M F. A scaled conjugate gradient algorithm for fast supervised learning. Neural Networks, 1993, 6(4): 525–533.

Biographies

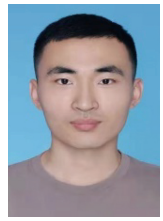

XIE Cunxiang was born in 1996. He received his B.S. degree in communication engineering from the Naval Aviation University, in 2019. He is currently pursuing his M.S. degree in information and communication engineering with the Department of Information Fusion, Naval Aviation University. His research interests include deep learning and specific emitter identification.
E-mail: 932304145@qq.com

ZHANG Limin was born in 1966. He received his Ph.D. degree in signal processing technology from Tianjin University, in 2005. Since 2005, he has been a professor with the Naval Aviation University. His research interests include satellite communication signal processing.
E-mail: iamzlm@163.com

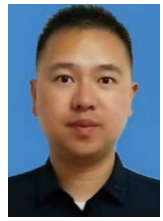

ZHONG Zhaogen was born in 1984. He received his Ph.D. degree in information and communication engineering from the Naval Aviation University, in 2013. He is currently an associate professor with the Naval Aviation University. His research interests include spread spectrum signal processing.
E-mail: zhongzhaogen@163.com